Size-dependent mechanical properties of axial and radial mixed AlN/GaN nanostructures

M.T. Hoang, Julien Yvonnet, Alexander Mitrushchenkov, Gilberte Chambaud, H.L. Duan

Size-dependent mechanical properties of axial and radial mixed AlN/GaN nanostructure

M.-T. Hoang[1]

[1]Université Paris-Est, MSME UMR 8208 CNRS, 5 Bd Descartes 77454 Marne-la-Vallée CEDEX 2, France.

E-mail: Minh-Tuan.Hoang@univ-paris-est.fr

J. Yvonnet[1]

[1]Université Paris-Est, MSME UMR 8208 CNRS, 5 Bd Descartes 77454 Marne-la-Vallée CEDEX 2, France.

E-mail: julien.yvonnet@univ-paris-est.fr

A. Mitrushchenkov[1]

[1]Université Paris-Est, MSME UMR 8208 CNRS, 5 Bd Descartes 77454 Marne-la-Vallée CEDEX 2, France

E-mail: alexander.mitrushchenkov@univ-paris-est.fr

G. Chambaud[1]

[1]Université Paris-Est, MSME UMR 8208 CNRS, 5 Bd Descartes 77454 Marne-la-Vallée CEDEX 2, France

E-mail: gilberte.chambaud@univ-paris-est.fr

H.L. Duan[2]

[2]Peking University, College of Engineering, State Key Laboratory for Turbulence and Complex Systems, Department of Mechanics and Engineering Science, CAPT, College of Engineering, Peking University Beijing 100871, China.

E-mail: hlduan@pku.edu.cn

Abstract. In this paper, continuum multiscale models are proposed to describe the size-dependent mechanical properties of two kinds of heterogeneous nanostructures: radially-heterogeneous nanowires and longitudinally-heterogeneous nanolaminates. In both cases, the continuum models involve additional surface/interface energies which allow capturing size effects. Several models of imperfect interface models, like coherent and spring-layer ones, are shown to respectively capture the size effects which are reported by first-principle calculations performed on heterogeneous nanostructures. In each case, a procedure is proposed to identify the parameters of the surface/interface model in the continuum framework, based on first-principles calculations performed on slab systems. The obtained continuum models allow avoiding full computations on atomistic models which are not affordable for large sizes (diameters, layer thickness).

An increase of the overall stiffness for both kinds of heterogeneous AlN/GaN nanostructures with the decrease of the dimensions is evidenced. The continuum models are then compared with full first principles calculations to demonstrate their accuracy and their ability to capture size effects.

PACS numbers: 62.23.Hj, 63.22.Np, 68.35.bg, 68.35.Ct, 68.35.Gy

Keywords: Surfaces, Interfaces, Nanowires, Nanolaminates, Size-effects, Mechanical properties

1. Introduction

Recently, the fabrication of axial/radial heterogeneous nanostructures like coated nanowires or nanolaminates has attracted special attention of the scientific community due to their multiple potential applications like energy harvesting devices. For example, Core/Multishell nanowire heterostructures have evidenced performances for high-efficiency light-emitting diodes [1], laser [2], high mobility electronic [3] and field effect transistors [4]. Such nanostructures can be fabricated by several processes like chemical vapour deposition [5] or MOCVD [3]. Tak et al. have demonstrated that ZnO/CdS core/shell heterostructures nanowire arrays can be used in high efficiency nanowire solar energy conversion devices [6]. Recently, Wong et al. have shown that the electron gases in core shell GaN/AlGaN nanowires have unusual properties compared to their bulk counterparts [7].

Besides these *radially*-heterogeneous nanostructures, more classical heterogeneous structures like laminates can show unusual properties when thickness of layers decreases to several nanometers, like giant dielectric constants [8], or improved mechanical and electrical properties [9, 10, 11, 12, 13, 14, 15, 16, 17]. For these materials it is strongly suggested that the unusual effects are originated from surface/interface.

Size-dependent behavior in nanostructures is usually modeled in the context of continuum mechanics by means of surface/interface additional energy, involving surface tension and stress effects in fluids and solids [18, 19, 20]. A classical continuum model to explain the surface effects on the elastic properties of nanostructures was formulated by Gurtin and Murdoch [21] and Murdoch [22] for materials interfaces. Later it was further applied by many researchers [23, 24, 25] to analyze the elastic properties of nanomaterials. Another widely used imperfect interface model is the spring layer elastic model, which has been utilized to model thin interphases or interfacial damage, and to estimate the effective elastic and thermoelastic moduli of particulate and fiber composites with imperfectly bounded interfaces [26, 27, 28, 25, 29, 30, 31, 32]. A general framework for defining imperfect interface models in a linear multiphysics context was recently provided [33].

In the present work, we focus on GaN-AlN axial/radial nanostructures, which were investigated in several recent studies for potential applications to optoelectronic devices with lower threshold current density, lower radiative recombination rate, lower emission spectra, and reduced sensitivity to temperature [34] as compared to their bulk counterparts. More specifically, it was shown that an AlN interlayer inserted between AlN/GaN barrier layer and the GaN channel improves the electron mobility by reducing alloy scattering [35, 36, 37, 38] and that the valence electron concentration had an influence on the elastic stiffness in such composites [39]. Elastic strain relaxation in AlN/GaN nanolaminates was calculated [34] and related interfaces were investigated by laser-assisted APT [40]. Thin Ti_3SiC_2 nanolaminates were investigated using theoretical first-principles calculations [41].

In this paper, the size-dependent elastic properties in radial (coated nanowires) and axial (nanolaminates) AlN/GaN nanostructures are investigated by first-principles computations. It is shown that these size effects are directly related to surface/interface effects at the nanoscale. Continuum models involving additional surface/interface energies are introduced to describe the nanostructures to avoid the high complexity of first principles calculations in the case of larger systems. Procedures to identify the parameters of the surface/interface models are provided. Comparisons between continuum models and full first-principles calculations are provided.

2. Continuum models

In this part, the considered heterogeneous nanostrucures are presented. The objective is to propose continuum models, able to capture size effects, to replace the fully atomistic models, which are highly computationally demanding, to solve when increasing the number of atoms, and able to capture the size effects.

2.1. Radially-heterogeneous nanowires

First, radially-heterogeneous AlN/GaN nanowires are considered. These structures are composed of a wurtzite AlN core with hexagonal section and 6 faces $[10\bar{1}0]$, periodic along the [0001]-direction, coated with a monolayer of GaN. (see Fig. 1).

It has been shown in previous works (see e.g. [42, 43, 44, 45]) that such structures show mechanical size effects, e.g. the effective stiffness of the nanowire depends on its radius and can increase significantly for diameters below 5 nm. In the present case, the nanostructure is heterogeneous, but the heterogeneity consists in a single layer of GaN. We propose to capture the effects of both surface effects related to the free surfaces and of the GaN shell by an effective surface in a Gurtin-Murdoch surface elasticity framework. Then, the nanostructure is replaced by a bulk structure made of AlN, coated by a surface which possesses its own behavior, in order to capture the mentioned size-effects. The equations of this model are presented as follows.

Let S be a surface in R^2. The projector operator $\mathbf{T}$ is introduced to define the

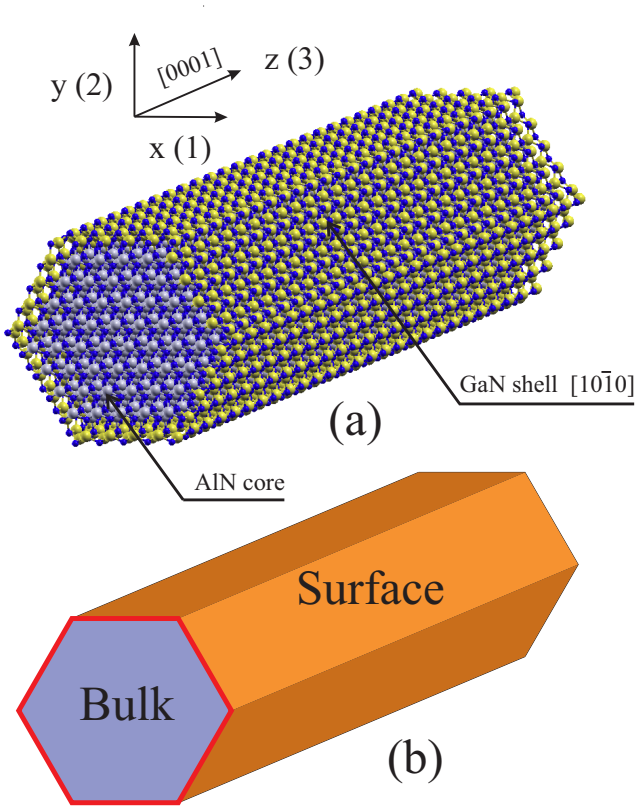

Figure 1. (a) First-principles model of radially-heterogeneous AlN/GaN nanowire. The blue, grey and yellow colors refer to N, Al and Ga atoms, respectively; (b) continuum model, consisting of bulk solid coated with an elastic surface.

projection on a plane tangent to S in a point $\mathbf{x} \in S$ by

$$T_{ij} = \delta_{ij} - n_i n_j \tag{1}$$

where δ_{ij} is the second-order identity tensor and n_i is the unitary vector normal to S in $x \in S$. Let $\mathbf{v}$ a vector and $\mathbf{A}$ a second-order tensor, then the projected vector $\mathbf{v}^s$ on the surface, and the surface second-order tensors A^s_{ij}, are defined respectively by:

$$v^s = T_{ij} v_j, \quad A^s_{ij} = T_{ik} A_{km} T_{mj} \tag{2}$$

Furthermore, if A_{ij} is differentiable, the surface divergence operator is defined as

$$A^s_{ij,j} = A_{ij,k} T_{kj} \tag{3}$$

The equations describing the equilibrium of a solid equipped with an elastic surface have been initially proposed by Gurtin and Murdoch [21]. Other justifications can be found e.g. in [46]. A body defined in a domain $\Omega \subset R^3$ with boundary $\partial\Omega$ is considered, with $S \subset \partial\Omega$. The equations of this model are summarized below:

$$\sigma_{ij,j} + f_i = 0, \quad \text{in} \quad \Omega \tag{4}$$

$$\sigma^s_{kj,i}T_{kj} + [[\sigma_{ij}n_j]] = 0, \quad \text{on } S \tag{5}$$

$$[[u]] = 0 \quad \text{on } S \tag{6}$$

where (4) is the bulk equilibrium equation, whereas (5) defines the surface equilibrium. In (4)-(5), σ_{ij} is the stress Cauchy second-order tensor, f_i is a body force vector, σ^s_{ij} is the surface stress tensor and $[[.]] = (.)^{(2)} - (.)^{(1)}$ is the jump between bulk and the interface. The assumption of a linear elastic behavior and of small perturbations are made. The constitutive laws for bulk and surface are given by

$$\sigma_{ij} = C_{ijkl}\varepsilon_{kl} \tag{7}$$

$$\sigma^s_{ij} = C^s_{ijkl}\varepsilon^s_{kl} + \tau^s_{ij} \tag{8}$$

In Eqs. (7) and (8), ε is the second-order strain tensor defined by $\varepsilon_{ij} = \frac{1}{2}(u_{i,j} + u_{j,i})$, C_{ijkl}, C^s_{ijkl} are the fourth-order elastic bulk and surface tensor, respectively and τ^s_{ij} denotes surface residual stress. It is worth noting that this form is a generalization of the Shuttleworth's law [47], the latest being restricted to isotropic surfaces. In the present work, the surfaces are fully anisotropic due to the wurtzite symmetries of the studied structures, which better justifies this model. Using (2), the surface stress and strain tensors are expressed by

$$\sigma^s_{ij} = T_{ik}\sigma_{km}T_{mj}, \qquad \varepsilon^s_{ij} = T_{ik}\varepsilon_{km}T_{mj} \tag{9}$$

Equations (4) - (5) are completed by Dirichlet and Neumann boundary conditions on portions of the external boundary $\partial\Omega_u$ and $\partial\Omega_F$, respectively, such that $\partial\Omega_u \cap \partial\Omega_F = \emptyset$, $\partial\Omega = \partial\Omega_u \cup \partial\Omega_F$:

$$\sigma_{ij}n_j = \overline{F}_i \quad \text{on} \quad S_F \tag{10}$$

$$u_i = \overline{u}_i \quad \text{on} \quad S_u \tag{11}$$

where u_i is the displacement vector, $\overline{u}_i$ is a prescribed displacement on the boundary S_u, and n_j is the outward normal vector to the external surface S. The surface is attached to the bulk through (6).

Adopting Voigt's notations, the strain and stress tensor components are denoted by: $[\sigma] = \{\sigma_{11}, \sigma_{22}, \sigma_{33}, \sigma_{23}, \sigma_{13}, \sigma_{12}\} = \{\sigma_1, \sigma_2, \sigma_3, \sigma_4, \sigma_5, \sigma_6\}$ and $[\varepsilon] = \{\varepsilon_{11}, \varepsilon_{22}, \varepsilon_{33}, 2\varepsilon_{23}, 2\varepsilon_{13}, 2\varepsilon_{12}\} = \{\varepsilon_1, \varepsilon_2, \varepsilon_3, \varepsilon_4, \varepsilon_5, \varepsilon_6\}$. Indices 1, 2 and 3 are associated to directions x, y and z, respectively. In this paper, the studied materials (ZnO, AlN, GaN) have a crystalline wurtzite structure. In this case, the elastic tensor is described by 5 independent constants $C_{11}, C_{12}, C_{13}, C_{33}$ and C_{44}. The matrix $\mathbf{C}$ associated to the fourth-order tensor C_{ijkl} and such that $[\sigma] = \mathbf{C}[\varepsilon]$ is then expressed by:

$$\mathbf{C} = \begin{bmatrix} C_{11} & C_{12} & C_{13} & 0 & 0 & 0 \\ C_{12} & C_{11} & C_{13} & 0 & 0 & 0 \\ C_{13} & C_{13} & C_{33} & 0 & 0 & 0 \\ 0 & 0 & 0 & C_{44} & 0 & 0 \\ 0 & 0 & 0 & 0 & C_{44} & 0 \\ 0 & 0 & 0 & 0 & 0 & \frac{C_{11}-C_{12}}{2} \end{bmatrix} \tag{12}$$

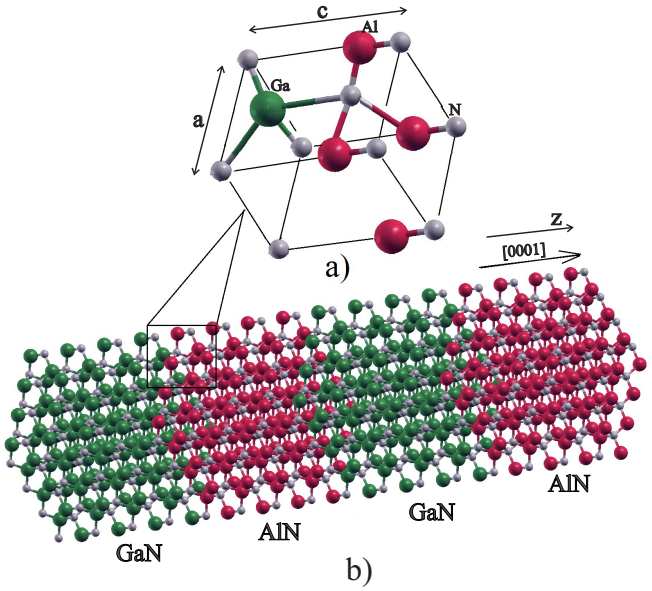

Figure 2. a) Wurtzite unit cell; b) AlN/GaN nanolaminates with 4 bilayers stratified on the [0001]-direction.

Table 1. Bulk lattice parameters a and c (in Å) and elastic parameters (in GPa) for wurtzite AlN and GaN.

Material	a	c	C_{11}	C_{33}	C_{13}	C_{12}	C_{44}
AlN	3.124	5.007	392.1	376.6	104.5	136.5	116
GaN	3.198	5.204	357.7	393.9	93.9	130.7	92.7

2.2. Nanolaminated heterogeneous structures

In the case of heterogeneous nanolaminates (layers of different materials in one direction, see Fig 3 (a), we propose a continuum model consisting of a periodic bi-material composite with parallel layers separated by an imperfect interfaces, in order to capture size effects. The microstructure is depicted in Fig. 3 (b), corresponding to an open domain $\Omega \subset R^3$ whose boundary is denoted by $\partial\Omega$.

A nanolaminate consisting of wurtzite AlN/GaN layers is considered. Each layer is initially constructed from a unit wurtzite cell (see Fig. 2), and repeated n times in the [0001]-direction, and infinitely in the other two orthogonal directions, as depicted in Fig. 2(b).

The AlN material is associated with phase (1), and GaN with phase (2). The layer (1) has a thickness $h = nc^{AlN}$ and the layer (2) has a thickness $L - h = nc^{GaN}$ (see Table 1). The layers are assumed to be separated by imperfect interfaces. From our first-principles observations, size-dependent elastic properties in the [0001]-direction (normal to the interface) have been observed. This motivates the use of a spring-layer imperfect interface model, which is described in the following. The equations of the model are given by:

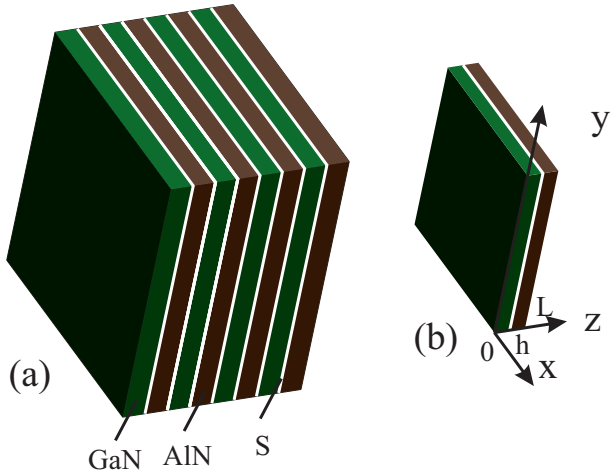

Figure 3. (a) Continuum model of nanolaminate consisting of periodic layers separated by an imperfect interface S; (b) associated continuum periodic elementary cell.

$$\sigma_{ij,j} = 0 \text{ in } \Omega \tag{13}$$

$$\sigma_{ij} = C^{(r)}_{ijkl}\varepsilon_{kl} \text{ in } \Omega \tag{14}$$

$$[[\sigma_{ij}n_j]] = 0 \text{ on } S \tag{15}$$

$$\sigma_{ij}n_j = C^{s}_{ij}[[u_j]] \text{ on } S \tag{16}$$

where σ_{ij} denotes the Cauchy stress tensor components, $C^{(r)}_{ijkl}$ are the elastic moduli of phase r, ε_{ij} denotes the linearized strain tensor components $\varepsilon_{ij} = \frac{1}{2}(u_{i,j} + u_{j,i})$ with u_i the displacements components, n_i is the unit vector normal to the interface Γ, $[[.]] = (.)^{(2)} - (.)^{(1)}$ is the jump of quantities across S, and C^{s}_{ij} refers to the surface stiffness moduli. The problem is completed by boundary conditions on $\partial\Omega$. Eq. (13) refers to the balance of momentum, while Eqs (15)-(16) are associated with the interfacial continuity conditions.

In absence of body forces and external traction, the related energy of the system is given by:

$$E = \int_V \frac{1}{2}\varepsilon_{ij}C^{(r)}_{ijkl}\varepsilon_{kl}dV + \int_S \frac{1}{2}[[u_i]]C^{s}_{ij}[[u_j]]d\Gamma \tag{17}$$

Identifying $C^{(1)}_{ijkl}$, $C^{(2)}_{ijkl}$, C^{s}_{ij}, Eqs. (13)-(16) with appropriate boundary conditions uniquely define the local displacement $u_i(z)$, strain $\varepsilon_{ij}(z)$ and stress $\sigma_{ij}(z)$ fields within each layer of the nanolaminate. An elementary cell is considered, as depicted in Fig. 3 (b), which is assumed to be subject to a homogeneous strain $\bar{\varepsilon}_{ij}$ through:

$$u_i = \bar{\varepsilon}_{ij}x_j + \tilde{u}_i \text{ on } \partial\Omega \tag{18}$$

where x_i is a coordinate in Ω and $\tilde{u}_i$ is a periodic function over Ω. For such a condition, Eqs. (13)-(16) can be solved in closed form and yield piece-wise linear components

of the displacements along the $z-$axis. The related constants can be determined by considering the boundary conditions (18) at $(z = 0)$ and $(z = L)$, and the continuity conditions (15)-(16) at $(z = h)$. In the case of AlN/GaN nanolaminates in the [0001]-direction, the elastic matrix for wurtzite is given in each phase by (12) and their values are provided in Table 1.

The interface stiffness tensor is assumed in the form:

$$\mathbf{C}^s = \begin{bmatrix} 0 & 0 & C^s_{13} \\ 0 & 0 & C^s_{23} \\ C^s_{13} & C^s_{23} & C^s_{33} \end{bmatrix} \tag{19}$$

For this case, the resulting displacement field expression is provided in the Appendix od section 7.

Given the displacement field $u_z(z)$ within the nanolaminate, a localization tensor $A_{ijkl}(z)$ can be constructed such that:

$$\varepsilon_{ij}(z) = A_{ijkl}(z)\overline{\varepsilon}_{kl} \tag{20}$$

Using the constitutive equation (14) and averaging over Ω, we obtain the effective constitutive law for the homogenized nanolaminate as:

$$\overline{\sigma}_{ij} = \overline{C}_{ijkl}\overline{\varepsilon}_{kl} \tag{21}$$

with $\overline{\sigma}_{ij} = \frac{1}{V}\int_\Omega \sigma_{ij}(z)d\Omega$ and

$$\overline{C}_{ijkl} = \frac{1}{V}\int_\Omega C^{(r)}_{ijmp}(z)A_{mpkl}(z)dV \tag{22}$$

with V the volume of Ω. We provide the expressions of the effective coefficients as follows:

$$\overline{C}_{33} = \frac{C^1_{33}C^2_{33}C^s_{33}L}{C^2_{33}C^s_{33}h + C^1_{33}\left(C^2_{33} + C^s_{33}\left[L-h\right]\right)} \tag{23}$$

$$\overline{C}_{13} = \frac{C^s_{33}\left(C^1_{13}C^2_{33}h + C^2_{13}C^1_{33}\left[L-h\right]\right)}{C^2_{33}C^s_{33}h + C^1_{33}\left(C^2_{33} + C^s_{33}\left[L-h\right]\right)} \tag{24}$$

$$\overline{C}_{44} = \frac{C^s_{13}C^1_{44}C^2_{44}L}{C^1_{44}C^2_{44} + C^s_{13}C^2_{44}h + C^s_{13}C^1_{44}\left(L-h\right)} \tag{25}$$

and

$$\overline{C}_{55} = \frac{C^s_{23}C^1_{44}C^2_{44}L}{C^1_{44}C^2_{44} + C^s_{23}C^2_{44}h + C^s_{23}C^1_{44}\left(L-h\right)} \tag{26}$$

We note that when C^s_{13}, C^s_{23} and C^s_{33} tend to infinity, corresponding to a perfectly bounded (infinitely rigid) interface, the effective coefficients tend to finite values corresponding to the behavior of the homogenized composite without imperfect interface.

3. Identification of surface/interface coefficients from first-principle calculations

3.1. Radially-heterogeneous nanowires

To evaluate the surface elastic coefficients C^s_{ijkl} and τ^s_{ij} in (8), the procedure described in details in [42, 43] is employed and briefly reviewed as follows. First-principles calculations are conducted on the CRYSTAL code [48] with the periodic DFT method. The employed basis sets are: 86-21G* for Al[49], 86-4111 d416 for Ga [50, 51] and G31 d16 for N [52]. The functional used in the calculations is PWGGA.

Firstly, we consider several slab models are consisting of n layers of AlN elementary cells, coated with a layer of a single elementary cell of GaN on its external surface (see Fig. 4). The elementary cell is repeated periodically in the x (1) and z (3) directions, Direction 3 corresponding to the growth direction of the nanowire (see Fig. 1).

The free surfaces correspond to $[10\bar{1}0]$ surfaces. Strains are prescribed along the plane (x, z) to compute the surface elastic coefficients and surface residual stress by the relationship:

$$C^{slab}_{ij} = \frac{1}{S}\frac{\partial^2 E^{slab}}{\partial\overline{\varepsilon}_i \partial\overline{\varepsilon}_j} \tag{27}$$

$$\tau^{slab}_{i} = \frac{1}{S}\frac{\partial E^{slab}}{\partial\overline{\varepsilon}_i} \tag{28}$$

were $S = ac$ is the area of an elementary cell. The derivatives are computed numerically by fitting a polynomial to several discrete points, corresponding to small increments (± 0.005) of the prescribed strain components. Let us note at that point that these coefficients are those of the complete slab system, including both bulk and surface energies (expressed in Hartree/atom), which allows to sum them:

$$E^{slab} = E^b + E^s \tag{29}$$

These coefficients do not correspond to the actual surface elastic coefficients:

$$C^{slab}_{ij} \neq C^s_{ij}, \quad \tau^{slab}_i \neq \tau^s_i \tag{30}$$

To separate surface and bulk energy contributions, we propose to conduct a series of several computations for different number of layers n. The following decomposition is introduced:

$$E^{slab}_i(w) = wE^s_i + (1-w)E^b_i \tag{31}$$

suggested by preliminary computations which have shown a linear dependency of coefficients C^{slab}_{ij} with respect to w, where w denotes the surface weight, defined as the ratio of surface atoms on the number of bulk atoms:

$$w = \frac{2}{n} \tag{32}$$

Eq. (31) can be rewritten as:

$$E_i^{slab}(w) = wE_i^s + (1-w)E_i^{slab}(w \to 0) \tag{33}$$

From (27), we obtain:

$$C_{ij}^{slab}(w) = wC_{ij}^s + (1-w)C_{ij}^{slab}(w \to 0) \tag{34}$$

where C_{ij}^s denote the surface elastic coefficients. Limit (bulk) values $C_{ij}^{slab}(w \to 0)$ can be computed from bulk coefficients by relaxing $\bar{\varepsilon}_2$ and by fixing ε_1 and ε_3. Minimizing the energy (see [42]) then leads to:

$$C_{11}^{slab}(w \to 0) = \frac{(C_{11}^b)^2 - (C_{12}^b)^2}{C_{11}^b} \tag{35}$$

$$C_{13}^{slab}(w \to 0) = \frac{C_{13}^b(C_{11}^b - C_{12}^b)}{C_{11}^b} \tag{36}$$

$$C_{33}^{slab}(w \to 0) = \frac{C_{33}^b C_{11}^b - (C_{13}^b)^2}{C_{11}^b} \tag{37}$$

$$C_{55}^{slab}(w \to 0) = C_{44}^b \tag{38}$$

The procedure consists in computing the values of $C_{ij}^{slab}(w)$ for several values of w (by increasing the number of layers n). The values computed numerically through first-principles calculations are then fitted by a linear function. Eq. (34) can be rewritten as:

$$C_{ij}^{slab}(w) = C_{ij}^{slab}(w \to 0) + w\ r \tag{39}$$

where r is the slope of the linear function which is given by

$$r = C_{ij}^s - C_{ij}^{slab}(w \to 0) \tag{40}$$

From the estimation of r, the expression of the surface elastic parameters can be established by

$$C_{ij}^s = r + C_{ij}^{slab}(w \to 0) \tag{41}$$

To evaluate the surface residual stress, the relationship is used:

$$\tau_i^{slab} = w\tau_i^s \tag{42}$$

To convert surface elastic coefficients from Hartree/atom into N/m, the following relationship can be used:

$$C(\text{N/m}) = C(\text{Hartree/atom}) * \frac{4}{S(\mathring{A}^2)} * 435.974 \tag{43}$$

Practically, the 4 elastic and the 2 stress coefficients (C_{11}^s, C_{13}^s, C_{33}^s, C_{55}^s, τ_1^s and τ_3^s) are obtained by conducting 3 computations associated with 3 deformation modes.

The values of the elastic parameters of the slab system as a function of the thickness are presented in Table 2.

After fitting data in Figs. 5 and 6 by a linear function, the parameters (C_{ij}^s and τ^s) in N/m are provided in Table 3.

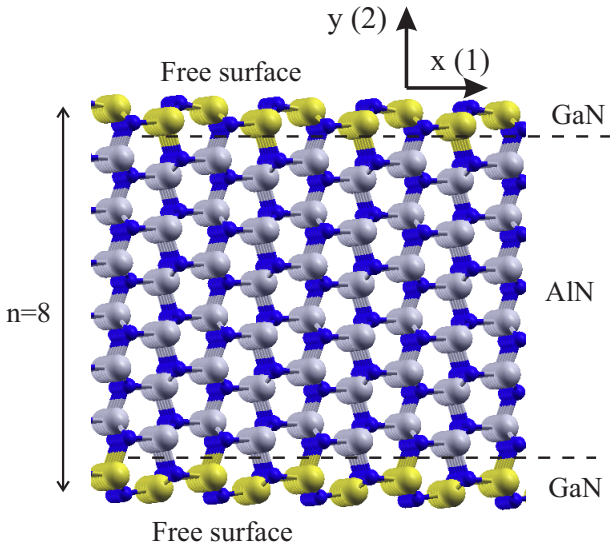

Figure 4. Slab model associated to an AlN surface coated with a monolayer of GaN, for $n = 8$ elementary cells in the layer. The blue, grey and yellow colors refer to N, Al and Ga atoms, respectively

Table 2. Effective elastic parameters of the slab system (in Hartree/atom), computed with PWGGA functional.

n	C_{11}^{slab}	C_{33}^{slab}	C_{13}^{slab}	C_{55}^{slab}	τ_1^{slab}	τ_3^{slab}
4	0.89356	0.72625	0.15994	0.29300	0.0220	0.0119
6	0.87580	0.76813	0.16258	0.28921	0.0146	0.0078
8	0.86656	0.78925	0.16331	0.28744	0.0110	0.0059
10	0.86097	0.80147	0.16390	0.28640	0.0088	0.0047
20	0.84998	0.82579	0.16503	0.28430	0.0044	0.0024
∞	0.8392	0.85115	0.1664	0.28205	0	0

Table 3. Surface parameters of the effective surface of AlN coated with a monolayer of GaN (in N/m).

	C_{11}^s	C_{33}^s	C_{13}^s	C_{55}^s	τ_1^s	τ_3^s
PWGGA	120.642	56.192	24.546	40.828	1.26	1.47

3.2. Nanolaminated structures

Given the bulk values C_{ij}^1 and C_{ij}^2 in (23), the interface parameters C_{ij}^s must be identified for the AlN/GaN nanolaminate. For this purpose, several bi-layers slab models are constructed, as depicted in Fig. 7, where each layer contains n elementary cell along the $z-$axis.

In the calculations, the following basis sets were used: 82-126 for Al, 86-4111 d416 for Ga and G-31 d16 for N the same procedure as in the case AlN/GaN radial. For DFT Hamiltonian, the PWGGA with exchange-correlation functional was chosen. The

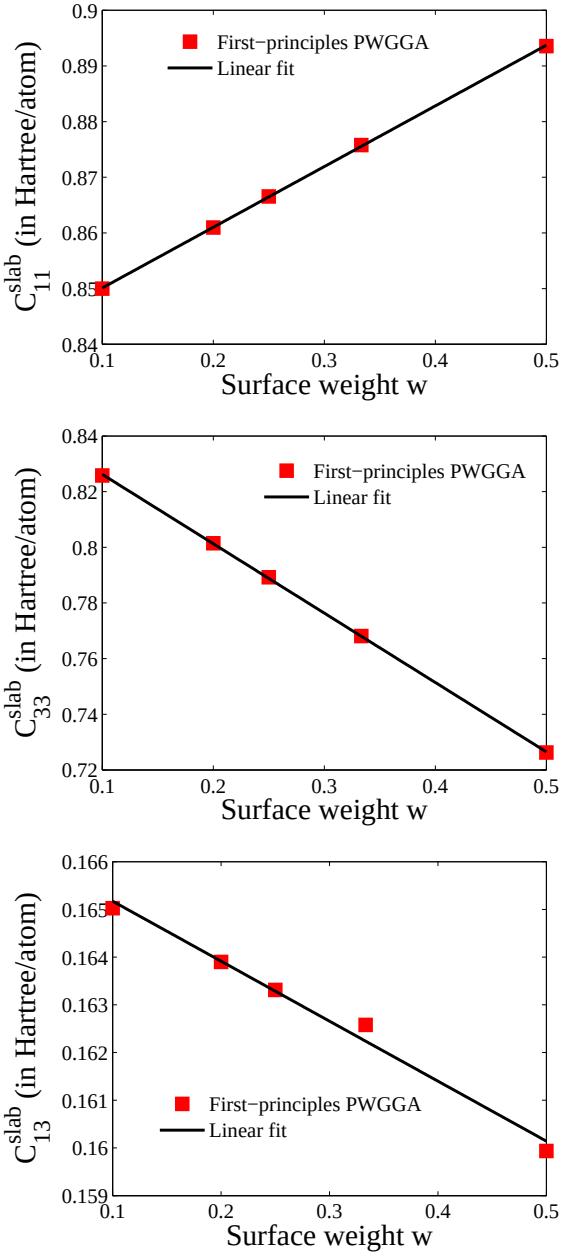

Figure 5. First-principles computed values of $C_{11}^{slab}, C_{33}^{slab}, C_{13}^{slab}$ and C_{55}^{slab} with respect to the surface weight (in Hartree/atom).

initial lattice parameters for AlN and GaN are reported in Table 1. Note that these parameters have rather close values for both materials. The effective elastic properties of the system are

$$\overline{C}_{ij}^{ab}(n) = \frac{1}{V}\frac{\partial^2 \overline{E}\,(\overline{\varepsilon})}{\partial \overline{\varepsilon}_i \partial \overline{\varepsilon}_j} \tag{44}$$

where $\overline{E}$ is the energy of the system for an overall prescribed strain $\overline{\varepsilon}$ and V denotes the volume of the slab. The calculated values for $\overline{C}_{ij}^{ab}(n)$ for $n = 2, 3, ..., 8$ are reported

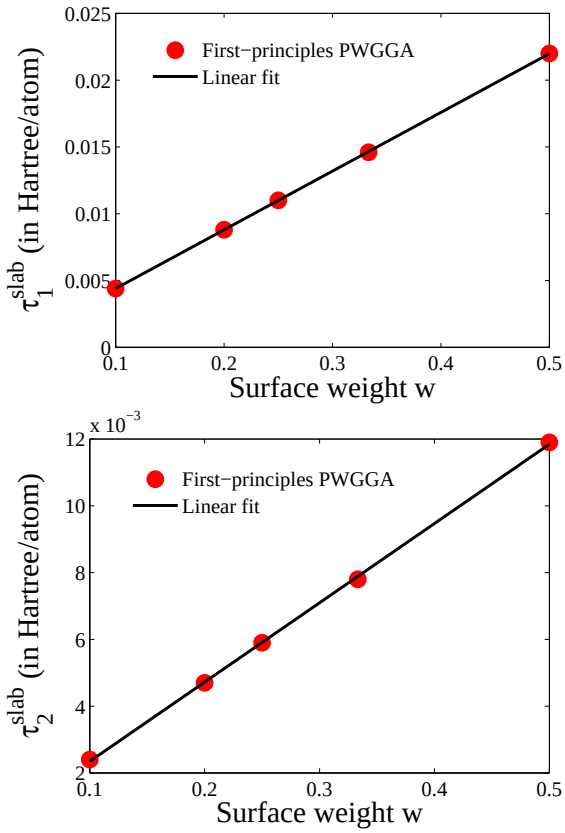

Figure 6. First-principles computed values of τ_1^{slab} and τ_3^{slab} with respect to the surface weight (in Hartree/atom).

Table 4. Overall elastic effective moduli (in GPa) of the composite using PWGGA functional.

n	$\overline{C}_{11}^{ab}$	$\overline{C}_{33}^{ab}$	$\overline{C}_{13}^{ab}$	$\overline{C}_{12}^{ab}$	$\overline{C}_{55}^{ab}$
2	374.7	388.8	99.2	135.7	102.5
3	374.6	387.4	99.7	135.8	102.7
4	374.6	387.0	99.8	135.8	102.8
5	374.5	386.7	99.9	135.7	102.8
6	374.5	386.6	99.9	135.8	102.9
8	374.4	386.0	100.0	135.7	102.9

in Table 4 and graphically depicted in Fig. 8.

We can note that the values of $\overline{C}_{ij}^{ab}$ depend on n and are thus size-dependent with respect to L, according to:

$$L = n\left(c^{AlN} + c^{GaN}\right) \tag{45}$$

The values of C_{33}^s, $C_{13}^s = C_{23}^s$ are then identified to fit the curves $\overline{C}_{ij}^{ab}(n)$ in Fig 8.

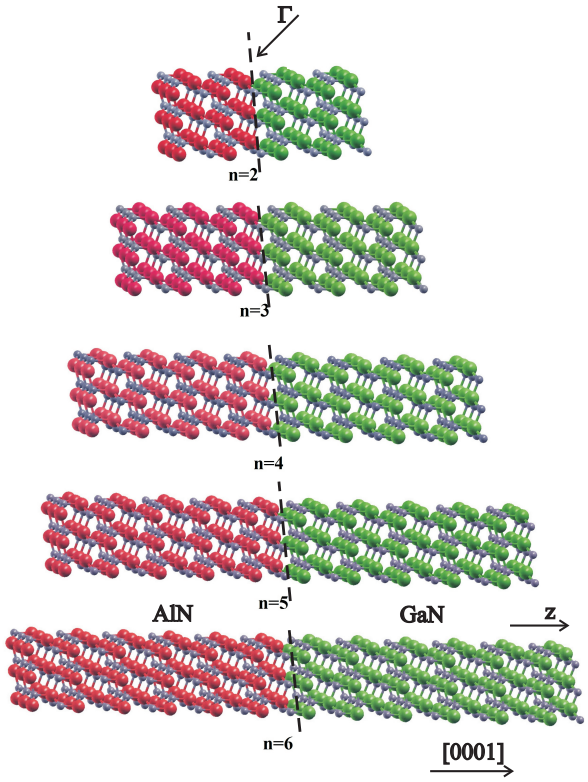

Figure 7. AlN/GaN nanolaminates comprising n cells in each layer.

Table 5. AlN/GaN interface stiffness parameters (in N/nm).

C^s_{13}	$4.879.10^4$
C^s_{33}	$-2.072.10^4$

The obtained values of the components are reported in Table 5.

We report negative values for the C^s_{33} coefficient, which is surprising at first glance. However, we provide an argument to explain it as follows. For the present spring layer model (23)-(26), the maximal stiffness $\overline{C}_{33}$ is obtained for a positive, infinite value of the interface coefficient C^s_{33}. Then, introducing an interface stiffness coefficient with any positive value can only reduce the effective stiffness. Nevertheless, in the present case, we have evidenced a stiffening effect by first-principles calculations associated with the interface, which can only occur for a negative value of the interface stiffness coefficient C^s_{33}. Note that negative values for interface elastic coefficients have been reported in other situations [53, 23, 54].

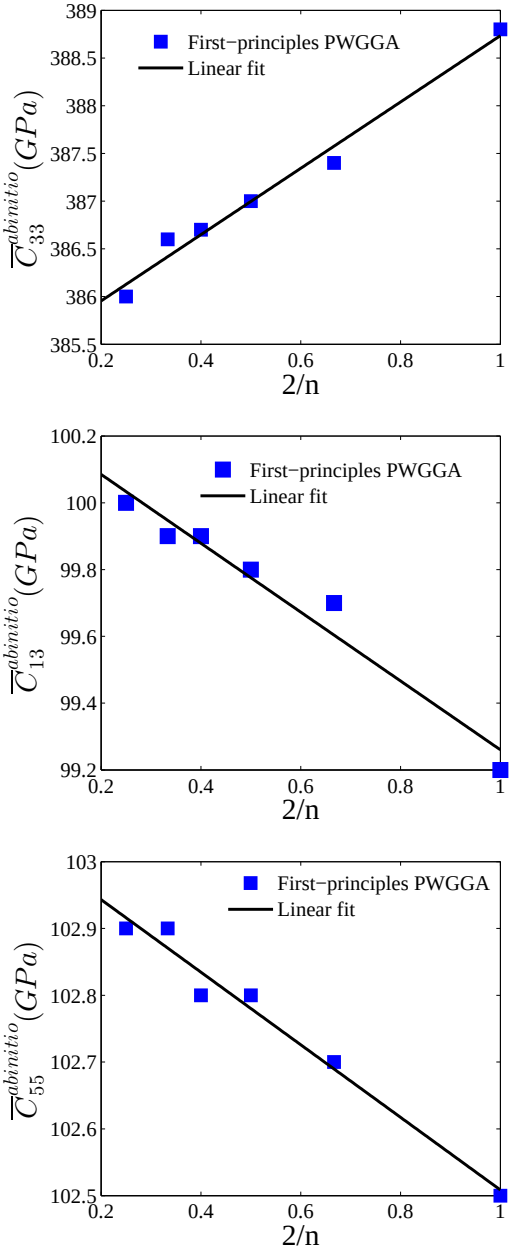

Figure 8. Effective elastic moduli $\overline{C}_{13}^{ab}$, $\overline{C}_{33}^{ab}$ and $\overline{C}_{55}^{ab}$ of the slab as function of $2/n$.

4. Validation and comparison between full computations and continuum models

4.1. Radially-heterogeneous nanowires

To validate the model, we have constructed several full continuum and atomistic models of AlN nanowires coated with a monolayer of GaN, comprising 108, 192, 300, 432, 588 and 768 atoms in one unit cell, corresponding to $n = 3, 4, 5, 6, 7, 8$ (see Fig. 9). Results with $(n-1)$ layers of AlN and one layer of GaN are provided in Table 6.

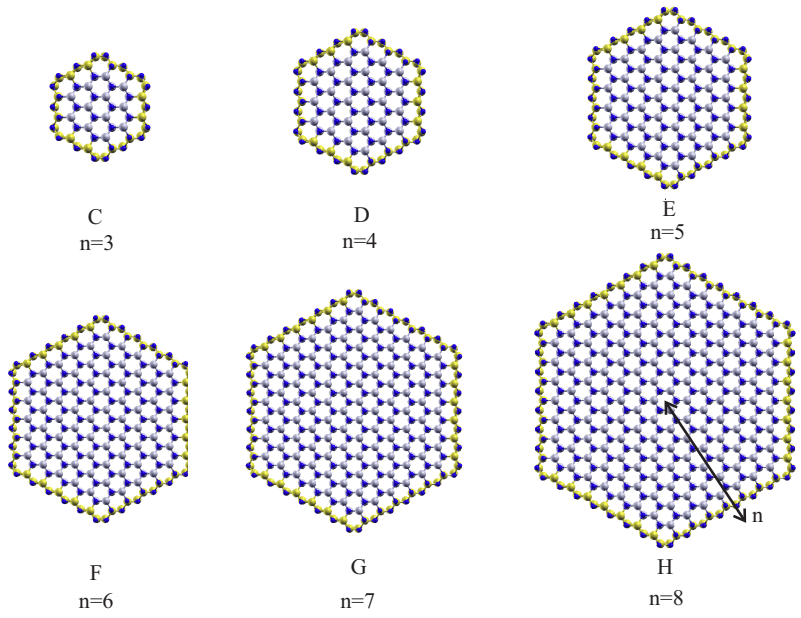

Figure 9. First-principles full models of radially-heterogeneous nanowires AlN/GaN for $n = 3, ..., 8$.

Table 6. Reference first-principles computations on radially-heterogeneous nanowires computed with PWGGA functional: overall $\bar{C}_{33}$ and Young's modulus coefficients, and relaxed value of the spacing constant c denoted by c_{opt}.

n	$N = 12n^2$	$\overline{C}_{33}$ (Hartree/atom)	Young modulus (GPa)	c_{opt} (Å)
3(C)	108	0.743880	586.234	5.128715
4(D)	192	0.756938	492.719	5.098882
5 (E)	300	0.766267	449.865	5.080366
6 (F)	432	0.772546	425.413	5.068043
7 (G)	588	0.777677	409.468	5.059255
8 (H)	768	0.747490	389.401	5.052847

The values of the effective Young modulus are provided in Table 6 as a function of the number of layers. The continuum model is described by Eqs. (4)-(5)-(6). The surface parameters are the one obtained by the procedure described in section 3.1. The continuum equations are solved by the finite element method (FEM) [43]. The FEM procedure has been implemented in a house-made code developed at MSME Lab and employs linear 4-node tetrahedral elements for the bulk, and 3-node surface elements for the boundary.

Results are presented in Fig. 10. A very good agreement between both models is noticed. The main advantage of the present continuum model is that is allows studying more complex configurations (loads, geometries) without limitations regarding sizes,

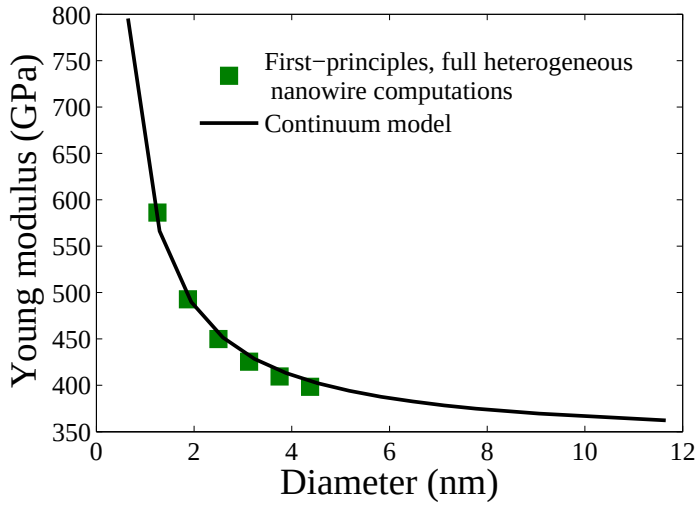

Figure 10. Comparison between heterogeneous nanowire fully described and solved by first-principles calculations and the continuum with equivalent surface energy for radially-heterogeneous AlN/GaN nanowires: effective Young modulus.

and with computational times which are of several order of magnitudes lower when solved with Finite Elements, as compared to full first-principles computations. In what follows,simulations using the FEM-continuum model are presented. Nanowires with the surface model identified above, equivalent to the radially-heterogeneous AlN/GaN nanowire with different diameters $d = 1$ nm, $d = 10$ nm and $d = 100$ nm are fixed at one end and are free to relax. Due to the surface residual stress, the nanowires deform, as shown in Figure 11. We can note that size effects are accurately captured, and vanish as expected when the diameter increases. It is worth noting that first-principles simulations of such configurations for diameters larger than a few nanometers cannot be afforded by most of nowadays computers.

We note that the present model is very satisfying for axial stretching of nanowires. The technique might also be applied when more than one layer of external coating is involved without modification in that case, but then volume elements might be more appropriate to model the coating. The proposed methodology could also be applied to surface elasticity introduced by roughness of the surface at the nanoscale (see e.g. [55, 56, 57]). However, in the case of bending, it has been shown that the Gurtin-Murdoch can introduce shortcomings. In that case, advanced surface elasticity theories might be required [58].

4.2. Nanolaminated structures

To evaluate the accuracy between our model and the first-principles calculations, we first compute the values of the effective coefficients $\overline{C}_{ij}$ as a function of L (or n, according to (45)). Results are reported in Fig 12, showing a good agreement between both models.

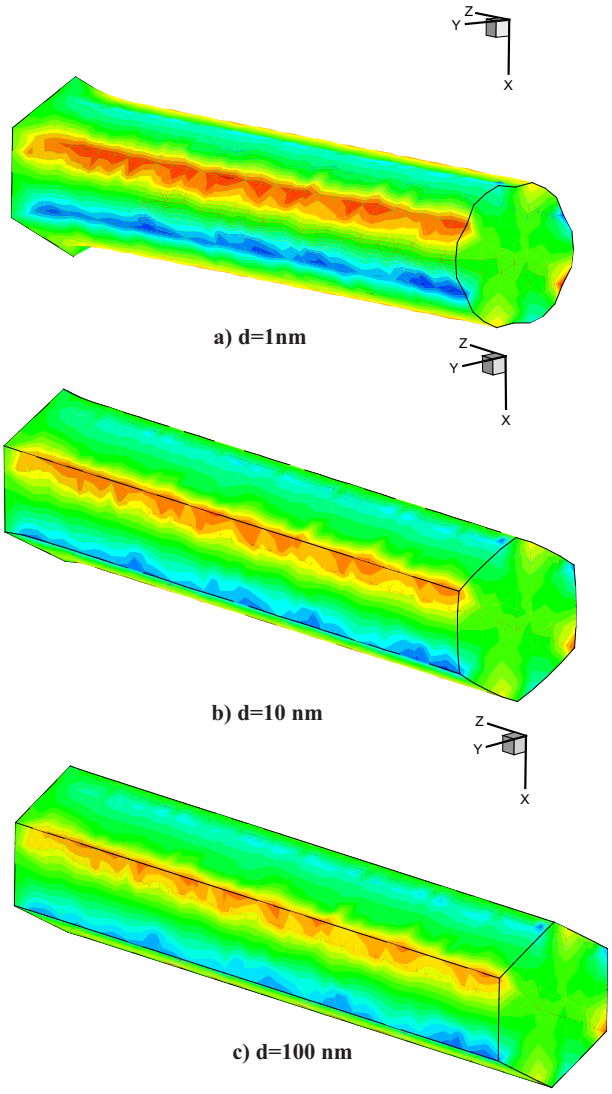

Figure 11. Magnified strain (10 times) in the heterogeneous nanowires fixed at one end for different diameters : a) $d = 1$ nm; b) $d = 10$ nm; c) $d = 100$ nm, simulated by FEM.

5. Conclusion

In this work, size effects on the mechanical properties of AlN/GaN heterogeneous nanostructures have been reported, namely in coated (core-shells) nanowires and nanolaminates. For both cases, first principles calculations have shown that these effects are directly related to the surface/interface effects. Continuum models have been proposed to replace the costly first-principles calculations while capturing accurately the size effects, as well as procedures to identify to surface coefficients. The comparisons between the continuum models and reference first-principles computations have proved a very good accuracy of the proposed models.

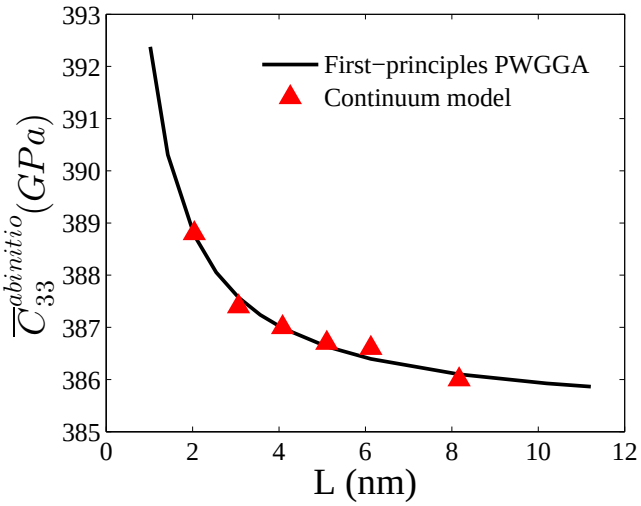

Figure 12. Effective elastic moduli of the AlN/GaN nanolaminate: comparison between the continuum model with imperfect interface and first-principles calculations.

6. Aknowledgements

The support J. Yvonnet enjoys for this work from Institut Universitaire de France (IUF) is gratefully aknowledged.

7. Appendix: expression of the $z-$component of the displacements in the nanolaminate

The closed-form of the $z-$component of the displacement field obtained by solving the problem (13)-(16) with continuity conditions (15) and (16) and boundary conditions (18) is provided as:

$$\begin{cases} u_z(z) = F_1' z, & z \in]0, h[\\ u_z(z) = E_2' + F_2' z, & z \in]h, L[\end{cases} \tag{46}$$

with

$$F_1' = \frac{C_{33}^2 C_{33}^s \overline{\varepsilon}_{33} L}{C_{33}^2 C_{33}^s h + C_{33}^1 \left(C_{33}^2 + C_{33}^s \left[L - h\right]\right)} \tag{47}$$

$$E_2' = \frac{\left(C_{33}^2 C_{33}^s h + C_{33}^1 \left[C_{33}^2 - C_{33}^s h\right]\right) \overline{\varepsilon}_{33} L}{C_{33}^2 C_{33}^s h + C_{33}^1 \left(C_{13}^2 + C_{33}^s \left[L - h\right]\right)} \tag{48}$$

and

$$F_2' = \frac{C_{33}^1 C_{33}^s \overline{\varepsilon}_{33} L}{C_{33}^2 C_{33}^s h + C_{33}^1 \left(C_{13}^2 + C_{33}^s \left[L - h\right]\right)} \tag{49}$$

References

[1] F. Qian, S. Gradecak, Y. Li, C.-Y. Wen, and C. M. lieber, Nano Lett. 5, 2287 (2005).
[2] F. Qian, S. Gradecak, Y. Li, H.-G. Park, Y. Dong, Y. Ding, Z. L. Wang and C. M. lieber, Nature material. 7, 701 (2008).
[3] M. J. Tambe, S. K. Lim, M. J. Smith, L. F. Allard, and S. Gradecak, Appl. Phys. Lett. 93, 151917 (2008).
[4] Y. He, Y. Zhao, C. Fan, J. Kang, R. Han and X. Liu, Electron Devices, IEEE Transactions on 56, 1199 (2009).
[5] L. J. Lauhon, M. S. Gudiksen, and D. Wang, Appl. Phys. Lett. 420, 57 (2002).
[6] Y. Tak, S. J. Hong, J. S. Lee, and K. Yong, J. Mater. Chem. 19, 5945 (2009).
[7] B. M. Wong, F. Lonard, Q. Li, and G. T. Wang, Nano Lett. 11, 3074 (2011).
[8] W. Li, O. Auciello, N. R. Premnath, and B. Kabius, Appl. Phys. Lett. 96, 162907 (2010).
[9] J. W. Elam, Z. A. Sechrist, and S. M. George, Thin Solid Films. 414, 43–55 (2002).
[10] M.-H. R. Jen, Y.-C. Tseng, and C.-H. Wu, Composites Science and Technology. 65, 775–779 (2005).
[11] P. Podsiadlo, Z. Tang, B. S. Shim, and N. A. Kotov, Nano Lett. 7, 1224–1231 (2007).
[12] D. Music, and M. J. Schneider, JOM. 59, 60–64 (2007).
[13] T.-J. Kang, J.-W. Yoon, D.-I. Kim, S.-S. Kum, Y.-H. Huh, Y.-H. Hahn, S. H. Moon, H.-Y. Lee, and Y. H. Kim, Adv. Mater. 19, 427–432 (2007).
[14] S. P. Fillery, H. Koerner, L. Drummy, E. Dunkerley, M. F. Durstock, D. F. Schmidt, and R. A. Vaia, ACS Appl. Mater. Interfaces. 4, 1388–1396 (2012).
[15] R. Venkatasubramanian, E. Siivola, T. Colpitts, and B. O'Quinn, Nature. 413, 597–602 (2001).
[16] Y.-W. Gao, and X.-D. Jia, J. Electron. Mater. 41, 552–559 (2012)
[17] L. Hultman, J. Bareno, A. Flink, H. Sderberg, K. Larsson, V. Petrova, M. Odn, J. E. Greene, and I. Petrov, Phys. Rev. B. 75, 155437 (2007).
[18] R. Shuttleworth, Proc. Phys. Soc. A. 63, 444 (1950).
[19] C. Herring, Structure and Properties of Solid Surfaces.The University of Chicago Press, Chicago (1953).
[20] J. Weissmller, and J. W. Cahn, Acta Mater. 45, 1899–1906 (1997).
[21] M. E. Gurtin, and A. I. Murdoch, Arch. Ration. Mech. Anal. 57, 291–323 (1975).
[22] A. I. Murdoch, Q. J. Mech. Appl. Math. 29, 245–275 (1976).
[23] R. E. Miller, and V. B. Shenoy, Nanotech. 11, 139–147 (2000).
[24] P. Sharma, S. Ganti, and N. Bhate, Appl. Phys. Lett. 82, 535–537 (2003).
[25] H. L. Duan, and B. L. Karihaloo, J. Mech. Phys. Solids. 55, 1036–1052 (2007).
[26] Y. Benveniste, Mech. Mater. 4, 197–208 (1985).
[27] G. W. Milton, The Theory of Composites. Cambridge University Press, Cambridge (2002).
[28] D. Shia, C. Y. Hui, S. D. Burnside, and E. P. Giannelis, Polymer Composites. 19, 608–617 (1998).
[29] Z. Hashin, Mechanics of Materials. 8, 333–348 (1990).
[30] Z. Hashin, J. Mech. Phys. Solids. 39, 745–762 (1991).
[31] Z. Hashin, J. Mech. Phys. Solids. 50, 2509–2537 (2002).
[32] Y. Benveniste, J. Mech. Phys. Solids. 54, 708–734 (2006).
[33] S. T. Gu, Q. C. He, J. Mech. Phys. 59(7), 1413 - 1426 (2011).
[34] A. D. Bykhovski, B. L. Gelmont, and M. S. Shur, J. Appl. Phys. 81, 6332 (1997).
[35] M. Miyoshi, H. Ishikawa, T. Egawa, K. Asai, M. Mouri, T. Shibata, M. Tanaka, and O. Oda, Appl. Phys Lett. 85, 1710–1712 (2004).
[36] L. Shen, S. Heikman, B. Moran, R. Coffie, N.-Q. Zhang, , D. Buttari, I. P. Smorchkova, S. Keller, S. P. DenBaars, and U. K. Mishra, IEEE Electron Device Lett. 22, 457–459 (2001).
[37] S. Keller, S. Heikman, L. Shen, I. P. Smorchkova, S. P. DenBaars, and U. K. Mishra, Appl. Phys. Lett. 80, 4387–4389 (2002).
[38] Y. Cao, and D. Jena, Appl. Phys. Lett. 90, 182112 (2007).
[39] J. Wang, and Y. Zhou, Phys. Rev. B. 69, 214111 (2004).

[40] B. Mazumder, M. H. Wong, C. A. Hurni, J. Y. Zhang, U. K. Mishra, and J. S. Speck, Appl. Phys. Lett. 101, 091601 (2012).
[41] J.-P. Palmquist, S. Li, P. O. A. Persson, J. Emmerlich, O. Wilhelmsson, H. Hgberg, M. I. Katsnelson, B. Johansson, R. Ahuja, O. Eriksson, L. Hultman, and U. Jansson, Phys. Rev. B. 70, 165401 (2009).
[42] A. Mitrushchenkov, G. Chambaud, J. Yvonnet and Q.-C. He, Nanotech. 21, 255702 (2010).
[43] J. Yvonnet, A. Mitrushchenkov, G. Chambaud and Q.-C. He, Comput. Meth. Appl. Mech. Eng. 200, 614-645 (2011).
[44] J. Yvonnet, A. Mitrushchenkov, G. Chambaud, Q.-C. He and S.-T. Gu, J. Appl. Phys. 111, 124305 (2012).
[45] M.-T. Hoang, J. Yvonnet, A. Mitrushchenkov, G. Chambaud, J. Appl. Phys. 113, 014309 (2013).
[46] T. Chen, M.-S. Chiu, C.-N. Weng, J. Appl. Phys. 100, 074308 (2006).
[47] R.C. Cammarata, Prog. Surf. Sci. 46, 1-38 (1994).
[48] R. Dovesi, V. R. Saunders, C. Roetti, R. Orlando, C. M. Zicovich-Wilson, F. Pascale, B. Civalleri, K. Doll, N. M. Marrison, I. J. Bush, Ph. D'Arco, and M. Llunell. CRYSTAL12 User's Manual. University of Torino, Torino (2012).
[49] B. Montanari, B. Civalleri, C. M. Zicovich-Wilson, R. Dovesi, Int. J. Quantum. Chem. 106, 1703-1714 (2006).
[50] J. E. Jaffe, Phys. Rev. B. 53, R4209 (1996).
[51] R. Pandeyyand, M. Causa', N.M. Harrison, M. Seel, J Phys.-Condens. Mat. 8, 3993-4000 (1996).
[52] C. Gatti, V. R. Saunders, C. Roetti, J. Chem. Phys. 101, 10686 (1994).
[53] V. B. Shenoy, Phys. Rev. B. 71, 094104 (2005).
[54] R. C. Cammarata, K. Sieradzki, and F. Spaepen, J. Appl. Phys. 87, 1227–1234 (2000).
[55] P. Mohammadi, and P. Sharma, Appl. Phys. Lett. 100, 133110 (2012).
[56] P. mohammadi, L.P. Liu, P. Sharma, and R.V. Kukta, J. Mech. Phys. Solids 61, 325-340 (2013).
[57] J. Weissmuller and H.L. Duan, Phys. Rev. Lett. 101, 146102 (2008).
[58] P. Chhapadia, P. Mohammadi, and P. Sharma, J. Mech. Phys. Solids 59(10), 2103-2115 (2013).